THE JOURNAL OF BIOLOGICAL CHEMISTRY
Vol. 274, No. 27, Issue of July 2, pp. 19329–19337, 1999

Printed in U.S.A.

Three-dimensional Structure of Guanylyl Cyclase Activating Protein-2, a Calcium-sensitive Modulator of Photoreceptor Guanylyl Cyclases*

(Received for publication, February 22, 1999, and in revised form, April 7, 1999)

James B. Ames‡§, Alexander M. Dizhoor¶‖, Mitsuhiko Ikura‡‡, Krzysztof Palczewski§§¶¶, and Lubert Stryer‖‖**

*From the ‡Center for Advanced Research in Biotechnology, University of Maryland Biotechnology Institute, Rockville, Maryland 20850, ¶Department of Ophthalmology/Kresge Eye Institute, Wayne State University School of Medicine, Detroit, Michigan 48201, **Division of Molecular and Structural Biology, Ontario Cancer Institute and Department of Medical Biophysics, University of Toronto, Toronto, Ontario, Canada M5G 2M9, §§Departments of Ophthalmology, Pharmacology, and Chemistry, University of Washington, Seattle, Washington 98195, and the ‖‖Department of Neurobiology, Stanford University School of Medicine, Stanford, California 94305-5125*

Guanylyl cyclase activating protein-2 (GCAP-2) is a Ca^{2+}-sensitive regulator of phototransduction in retinal photoreceptor cells. GCAP-2 activates retinal guanylyl cyclases at low Ca^{2+} concentration (<100 nM) and inhibits them at high Ca^{2+} (>500 nM). The light-induced lowering of the Ca^{2+} level from ~500 nM in the dark to ~50 nM following illumination is known to play a key role in visual recovery and adaptation. We report here the three-dimensional structure of unmyristoylated GCAP-2 with three bound Ca^{2+} ions as determined by nuclear magnetic resonance spectroscopy of recombinant, isotopically labeled protein. GCAP-2 contains four EF-hand motifs arranged in a compact tandem array like that seen previously in recoverin. The root mean square deviation of the main chain atoms in the EF-hand regions is 2.2 Å in comparing the Ca^{2+}-bound structures of GCAP-2 and recoverin. EF-1, as in recoverin, does not bind calcium because it contains a disabling Cys-Pro sequence. GCAP-2 differs from recoverin in that the calcium ion binds to EF-4 in addition to EF-2 and EF-3. A prominent exposed patch of hydrophobic residues formed by EF-1 and EF-2 (Leu^{24}, Trp^{27}, Phe^{31}, Phe^{45}, Phe^{48}, Phe^{49}, Tyr^{81}, Val^{82}, Leu^{85}, and Leu^{89}) may serve as a target-binding site for the transmission of calcium signals to guanylyl cyclase.

The calcium ion (Ca^{2+}) in retinal rod cells plays a critical role in regulating the recovery phase of visual excitation and adaptation to background light (1–4). Ca^{2+} enters rod outer segments through cGMP-gated cation-specific channels in the plasma membrane. These channels are kept open in the dark by the binding of cGMP. Light triggers the hydrolysis of cGMP, leading to channel closure. The cytosolic Ca^{2+} level decreases following illumination from ~500 to ~50 nM (5–7), because channel closure blocks the entry of Ca^{2+}, whereas its extrusion by a light-independent Na^+/K^+, Ca^{2+} exchanger continues (8). The light-induced lowering of the Ca^{2+} level promotes restoration of the dark state by stimulating the synthesis of cGMP (9). cGMP is synthesized in retinal photoreceptor cells by two membrane guanylyl cyclases, RetGC-1 and RetGC-2 (10–12).

Photoreceptor guanylyl cyclases are regulated by homologous Ca^{2+}-sensing proteins, guanylyl cyclase activating protein-1, -2, and -3 (GCAP-1, GCAP-2, and GCAP-3)[1] (13–15). Mammalian GCAP-1, GCAP-2, and GCAP-3 activate guanylyl cyclase at low Ca^{2+} (<100 nM). GCAP-2 in addition inhibits cyclase at high Ca^{2+} (16). In frogs, a GCAP homolog called guanylyl cyclase inhibitory protein (GCIP) inhibits cyclase at high Ca^{2+} (17). The amino acid sequences of GCAP-1, GCAP-2, GCAP-3, and GCIP (Fig. 1) showed that they are members of the EF-hand superfamily of Ca^{2+}-binding proteins (18). They are similar in sequence to recoverin (19), a retinal rod outer segment protein that inhibits rhodopsin kinase at high Ca^{2+} (20, 21). The recoverin branch of the EF-hand superfamily includes neuronal Ca^{2+} sensors such as neurocalcin, frequenin, visinin, and hippocalcin (reviewed in Ref. 22). Indeed, there is a homolog in yeast,[2] indicating that these calcium sensors arose early in the evolution of eukaryotes. The members of this family have a myristoylated amino terminus and four EF-hands. They all contain a Cys-Pro sequence in EF-1 that prevents Ca^{2+} binding by this EF-hand. The three-dimensional structures of the myristoylated and unmyristoylated forms of recoverin in the Ca^{2+}-free and Ca^{2+}-bound states have been determined by x-ray crystallography (24) and nuclear magnetic resonance (NMR) spectroscopy (25, 26). A striking feature of these structures is the large Ca^{2+}-induced conformational change. The binding of Ca^{2+} to recoverin leads to the extrusion of its myristoyl group, which is highly sequestered in the Ca^{2+}-free state, and to a large rotation of the two domains of the protein. The Ca^{2+}-induced exposure of the myristoyl group, termed the calcium-myristoyl switch, enables recoverin to bind to membranes at high Ca^{2+} (27, 28).

* This work was supported by Grants EY12347 (to J. B. A.), EY11522 (to A. M. D.), EY08061 (to K. P.), EY02005, and GM24032 (to L. S.) from the National Institutes of Health and the Medical Research Council of Canada (to M. I.). The costs of publication of this article were defrayed in part by the payment of page charges. This article must therefore be hereby marked "*advertisement*" in accordance with 18 U.S.C. Section 1734 solely to indicate this fact.

The atomic coordinates and structure factors (code 1jba.pdb) have been deposited in the Protein Data Bank, Brookhaven National Laboratory, Upton, NY.

‖ Recipient of a Career Development Award from Research to Prevent Blindness.

‡‡ Howard Hughes Medical Institute international research scholar.

¶¶ Recipient of a Jules and Doris Stein Professorship from Research to Prevent Blindness.

§ To whom correspondence should be addressed: Center for Advanced Research in Biotechnology, 9600 Gudelsky Dr., Rockville, MD 20850. Tel.: 301-738-6120; Fax: 301-738-6255; E-mail: james@carb.nist.gov.

[1] The abbreviations used are: GCAP, guanylyl cyclase activating protein; GCIP, guanylyl cyclase inhibitory protein; RMS, root mean square; HSQC, heteronuclear single quantum coherence.

[2] K. Devlin, C. M. Churcher, B. G. Marrell, M. A. Rajandream, and S. V. Walsh, unpublished data (locus NCS1SCHPO, Swiss-Prot accession no. Q09711).

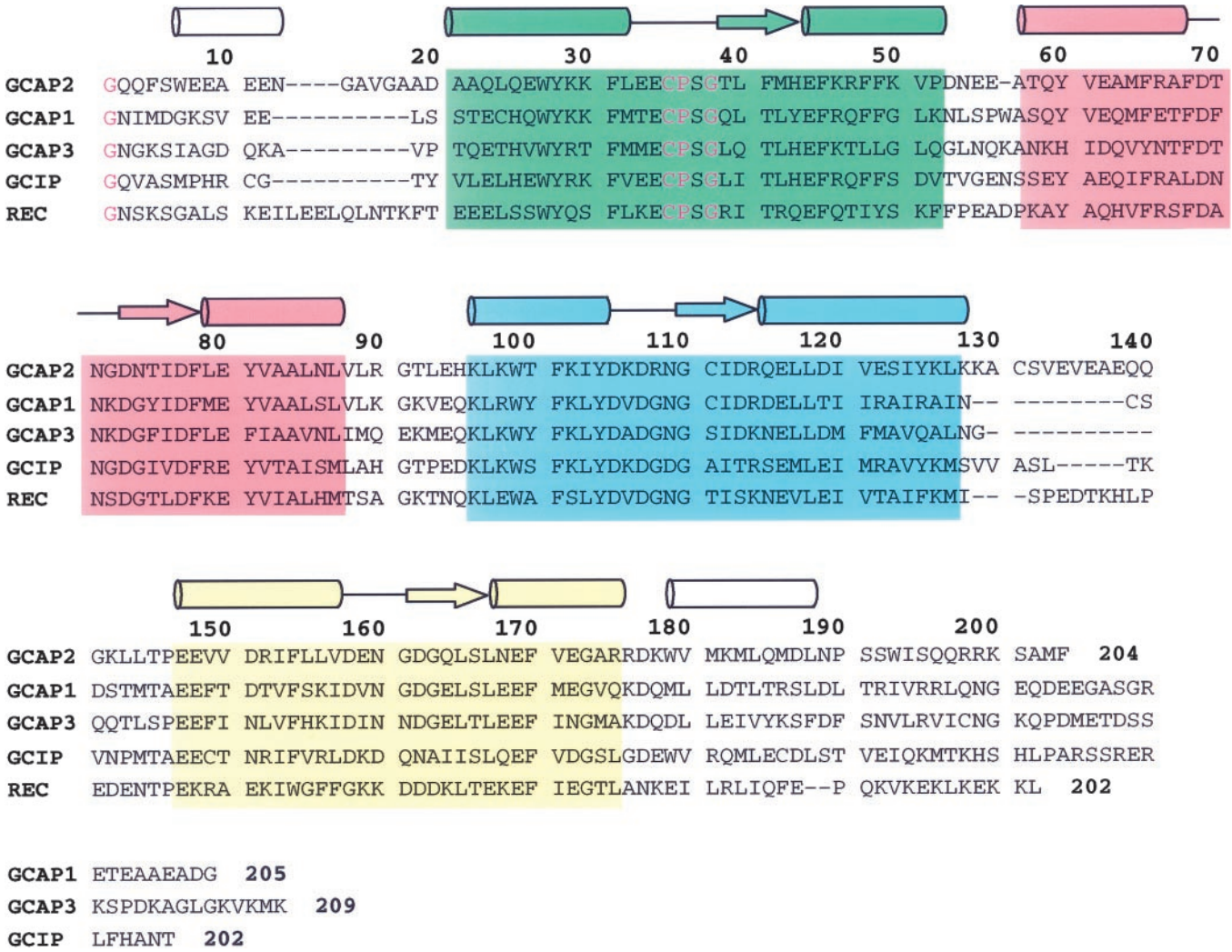

FIG. 1. **Amino acid sequence alignment of bovine GCAP-2 (accession no. U32856) with bovine GCAP-1 (accession no. P46065), human GCAP-3 (accession no. AF110002), frog GCIP (accession no. AF047884), and bovine recoverin (accession no. P21457).** The 29-residue EF-hand motifs are highlighted in color: *green*, EF-1; *red*, EF-2; *cyan*, EF-3; *yellow*, EF-4 . Regions of regular secondary structure (α-helices and β-strands) are indicated schematically.

We report here NMR spectroscopic studies of the three-dimensional structure of the Ca^{2+}-bound form of GCAP-2 as a step toward understanding the molecular mechanism of regulation of photoreceptor guanylyl cyclases. Ideally, one would like to solve the structures of the Ca^{2+}-free and Ca^{2+}-bound form of myristoylated GCAP-2, the physiologic species, but this is not yet feasible because of the low solubility of the myristoylated protein. We chose instead to solve the structure of Ca^{2+}-bound unmyristoylated GCAP-2, which is soluble and gives clearly resolved NMR spectra. Moreover, the structure of the unmyristoylated form of GCAP-2 is likely to be biologically pertinent. Unmyristoylated GCAP-2 is nearly as effective as myristoylated GCAP-2 in activating guanylyl cyclase at low Ca^{2+} and inhibiting it at high Ca^{2+} (29). Hence, structural studies of unmyristoylated GCAP-2 should reveal the Ca^{2+}-induced conformational changes underlying its regulation of cyclase.

EXPERIMENTAL PROCEDURES

Sample Preparation—Unmyristoylated recombinant GCAP-2 protein uniformly labeled with nitrogen-15 and carbon-13 was expressed in *Escherichia coli* strain BL21(DE3)pLysS using pET11d vector (Novagen) grown in M9 minimal medium (containing ^{15}N-labeled NH_4Cl and [$^{13}C_6$]glucose) according to previously published procedures (29). Specific labeling of GCAP-2 with valine or leucine, whose methyl carbons were stereospecifically labeled with ^{13}C, was prepared as described previously (30). Recombinant GCAP-2 protein expressed in *E. coli* forms insoluble inclusion bodies that were conveniently isolated and solubilized using 8 M urea (29). The urea-solubilized protein was then dialyzed extensively to remove urea. More than 80% of the refolded GCAP-2 (after dialysis of urea) remained soluble. The soluble GCAP-2 was then further purified using gel filtration chromatography described previously (29). In addition, anion-exchange chromatography (DEAE-Sepharose, Amersham Pharmacia Biotech) was performed at pH 6.1 and at room temperature. GCAP-2 eluted from the DEAE-Sepharose column (50-ml bed volume) using a salt gradient (0–0.5 M KCl over 60 min at flow rate, 2 ml min^{-1}).

Samples for NMR experiments were prepared by dissolving ^{15}N-labeled or $^{13}C/^{15}N$-labeled GCAP-2 (1 mM) in 0.5 ml of a 95% H_2O, 5% ^2H_2O or 99% ^2H_2O solution containing 50 mM KCl, 10 mM $CaCl_2$, 10 mM [$^2H_{10}$]dithiothreitol, 25 mM [$^2H_{28}$]octyl β-glucoside at pH 6.8.

NMR Spectroscopy—All NMR experiments were performed at 45 °C on a Varian UNITY-plus 500 or UNITY-600 spectrometer equipped with a four channel interface and a triple resonance probe with an actively shielded z gradient together with a pulse field gradient accessory.

The ^{15}N-^1H HSQC spectra (Fig. 2) (and heteronuclear multiple quantum coherence-J) were recorded on the uniformly ^{15}N-labeled GCAP-2 sample (95% H_2O, 5% ^2H_2O). The number of complex points and acquisition times were 256, 180 ms (^{15}N (F_1)) and 512, 64 ms (^1H (F_2)).

The exchange rates of amide protons were measured as described previously (31) by recording a series of ^{15}N-^1H HSQC spectra at various times (5, 40, 80, 200, 500, and 1000 min) after dissolving lyophilized protein in ^2H_2O.

All triple resonance experiments were performed as described previously (31) on the uniformly $^{13}C/^{15}N$-labeled GCAP-2 sample in 95% H_2O with the following number of complex points and acquisition times: HNCO (^{15}N (F_1) 32, 23.7 ms; ^{13}CO (F_2) 64, 42.7 ms; ^{1}H (F_3) 512, 64 ms), HNCACB (^{15}N (F_1) 32, 23.7 ms; ^{13}C (F_2) 48, 6.3 ms; ^{1}H (F_3) 512, 64 ms), CBCACONNH (^{15}N (F_1) 32, 23.7 ms; ^{13}C (F_2) 48, 6.3 ms; ^{1}H (F_3) 512, 64 ms), CBCACOCAHA (^{13}C (F_1) 52, 6.8 ms; ^{13}CO (F_2) 64, 42 ms; ^{1}H (F_3) 384, 64 ms), and HBHACONNH (^{15}N (F_1) 32, 23.7 ms; $^{1}H_{ab}$ (F_2) 64 21 ms; ^{1}H (F_3) 512, 64 ms). The triple resonance spectra were analyzed as described previously (31) and provided a nearly complete sequence-specific assignment of the backbone resonances.

The side chain resonances were assigned as described (30) by analyzing three-dimensional HCCH-total correlation spectroscopy spectra (7 and 14 ms mixing time) recorded on $^{13}C/^{15}N$-labeled GCAP-2 (99% $^{2}H_2O$) with the following number of complex points and acquisition times: ^{1}H (F_1) 128, 36.5 ms; ^{13}C (F_2) 32, 10.6 ms; ^{1}H (F_3) 416, 52 ms.

Structure calculations from residues 2–190 were performed using the YASAP protocol (32) within X-PLOR (33) as described previously (34). A total of 1791 interproton distance restraints (552 intraresidue, 455 sequential, 280 short range, and 350 long range) was obtained as described (30) by the analysis of ^{13}C-edited (and ^{15}N-edited) nuclear Overhauser effect spectroscopy-HSQC spectra (100 ms mixing time) recorded on $^{13}C/^{15}N$-labeled GCAP-2 (in 99% $^{2}H_2O$ for ^{13}C-edited experiments) or ^{15}N-labeled GCAP-2 (in 95% H_2O for ^{15}N-edited) with the following number of complex points and acquisition times: ^{1}H (F_1) 128, 25.6 ms; ^{13}C (F_2) 32 10.6 ms; ^{15}N (F_2) 32, 23.7 ms; ^{1}H (F_3) 416, 52 ms. In addition to the nuclear Overhauser effect-derived distance restraints, 18 distance restraints involving Ca^{2+} bound to loop residues 1, 3, 5, 7, and 12 in EF-2, EF-3, and EF-4 (24, 35, 36); 136 distance restraints for 68 hydrogen bonds; and 216 dihedral angle restraints (114 ϕ and 102 ψ) were included in the structure calculation. 50 independent structures were calculated, and 22 of those with the lowest total energy were selected. The average total and experimental distance energies are 4083 and 65 kcal mol^{-1} (calculated with the use of square-well potentials with a force constant of 50 kcal mol^{-1} Å^2). None of the distance and angle restraints were violated by more than 0.40 Å and 4.0°. The average root mean square (RMS) deviations from an idealized geometry for bonds, angles, and impropers are 0.00731 Å, 2.04°, and 0.91°, respectively.

Ca^{2+}-binding Measurements—Tryptophan fluorescence titrations (Fig. 3) were performed with 1 μM GCAP-2 in 2 ml of 0.1 M KCl, 50 mM HEPES (pH 7.5), 1 mM dithiothreitol at 25 °C. The free calcium concentration (30 nM to 2 μM) was set using an EGTA buffer system. The protein samples initially contained an equal molar ratio of total Ca^{2+} and EGTA (2 mM); the free Ca^{2+} concentration was adjusted by adding aliquots of 0.1 M EGTA. The free Ca^{2+} concentration was calculated based on the total amount of Ca^{2+} and EGTA present using the computer algorithm by Brooks and Storey (37). The calculated free Ca^{2+} concentrations agreed closely with measured Ca^{2+} concentrations using fluorescent indicator dyes fluo-3 and rhod-2 (Molecular Probes, Eugene, OR) with K_d of 0.4 and 1.0 μM, respectively (38).

Ca^{2+}-binding curves (Fig. 3) were obtained by the equilibrium dialysis method using a Dispo-equilibrium Biodialyzer (Sialomed, Columbia, MD). The apparatus consisted of two fluid-containing chambers (protein and buffer chambers) separated by a thin dialysis membrane (molecular mass cutoff, 10 kDa). The protein chamber contained 100 μl of 50 μM GCAP-2 in the same buffer used in the fluorescence titration above plus the addition of 1 μM $^{45}Ca^{2+}$ (total radioactivity, 1.4 μCi). The buffer chamber contained 100 μl of buffer (excluding any GCAP-2) plus the addition of a known amount of cold Ca^{2+}. The fluid in the two chambers was allowed to come to equilibrium after 12 h at 25 °C. Fifteen different dialysis experiments were performed at various cold Ca^{2+} concentrations (0, 1, 2, 10, 20, 25, 35, 45, 65, 100, 125, 140, 150, 160, 170 μM). At equilibrium, the free Ca^{2+} concentration is defined by

$$Ca^{2+}_{free} = Ca^{2+}_{tot}\left(\frac{r_b}{r_p}\right) \quad \text{(Eq. 1)}$$

where $Ca_{tot}{}^{2+}$ is the total Ca^{2+} concentration in the system, r_b is the radioactivity (counts/min) of $^{45}Ca^{2+}$ measured from an aliquot of the buffer chamber, and r_p is the radioactivity measured from an equal aliquot of the protein chamber. The concentration of Ca^{2+} bound to protein is as follows.

$$Ca^{2+}_{bound} = Ca^{2+}_{tot} - Ca^{2+}_{free} \quad \text{(Eq. 2)}$$

The fractional saturation is then defined as

$$Y = \frac{P_{bound}}{P_{tot}} = \frac{(Ca^{2+}_{free})^{\alpha}}{(Ca^{2+}_{free})^{\alpha} + K_d^{\alpha}} \quad \text{(Eq. 3)}$$

where P_{tot} is the total protein concentration in the system, P_{bound} is the concentration of protein species bound by Ca^{2+}, α is the Hill coefficient, and K_d is the apparent dissociation constant.

RESULTS

The structure of recombinant GCAP-2 uniformly labeled with carbon-13 and nitrogen-15 was studied by heteronuclear NMR spectroscopy. Two-dimensional heteronuclear single quantum coherence (^{15}N-^{1}H HSQC) NMR spectra, which serve as fingerprints of the conformation of main chain and side chain amide groups, were obtained. The HSQC spectra of unmyristoylated GCAP-2 are presented in Fig. 2. The Ca^{2+}-bound unmyristoylated protein exhibits many sharp and well resolved peaks. In contrast, the Ca^{2+}-free form exhibits broad and poorly resolved peaks, suggesting that Ca^{2+}-free GCAP-2 may represent an unfolded, aggregated protein. However, circular dichroism studies (data not shown) indicate that Ca^{2+}-free GCAP-2 is well folded with greater than 60% helical content. In addition, the Ca^{2+}-free GCAP-2 sample used in the NMR study is biologically active and was shown to activate photoreceptor guanylate cyclase. Hence, Ca^{2+}-free GCAP-2 in our study represents a well defined and folded protein. The observed broadening of the NMR peaks suggests that Ca^{2+}-free GCAP-2 most likely forms a dimer or other multimeric species under the conditions of the NMR experiment. The HSQC spectrum of Ca^{2+}-free myristoylated protein (data not shown) is similar to that of Ca^{2+}-free unmyristoylated protein. The low solubility of the Ca^{2+}-bound myristoylated protein prevented us from obtaining its HSQC spectrum.

The striking Ca^{2+}-induced spectral differences point to a large Ca^{2+}-induced structural change in the unmyristoylated protein. The characteristic NMR peaks of the Ca^{2+}-bound form saturate on addition of three molar equivalents of Ca^{2+} to the protein. Ca^{2+}-binding measurements using equilibrium dialysis and tryptophan fluorescence titrations also showed that three Ca^{2+} bind to unmyristoylated GCAP-2 (Fig. 3). The apparent affinity is 300 ± 40 nM, and the Hill coefficient is 2.1 ± 0.2. A stoichiometry of three Ca^{2+} bound to GCAP-2 is also supported by site-directed mutagenesis studies of the EF-hand motifs (16). Substituting glutamine for glutamate at position 12 of the EF-hand loops (EF-2, EF-3, EF-4) prevents the binding of Ca^{2+} and produces a constitutively active form of GCAP-2.

The strong and well resolved peaks observed in the HSQC spectrum of Ca^{2+}-bound, unmyristoylated GCAP-2 (Fig. 2*B*) suggested that it would be feasible to determine its three-dimensional structure. To elucidate the structure, resonances in the NMR spectrum were assigned to specific amino acid residues. Triple resonance experiments correlating ^{15}N, ^{13}C, and ^{1}H were performed to facilitate making assignments. Over 95% of the backbone resonances were assigned as indicated in Fig. 2*B*. These backbone assignments served as the basis for assigning about 80% of the side chain resonances. Nuclear Overhauser effect spectroscopy experiments were analyzed to establish nearly 2000 proton-proton distance relationships (~11 nuclear Overhauser effects/residue) throughout the protein. In addition, 216 dihedral angle restraints (ϕ and ψ) were deduced from J-coupling and chemical shift data. Finally, the three-dimensional structure was calculated by distance geometry and restrained molecular dynamics.

A superposition of 22 structures of Ca^{2+}-bound unmyristoylated GCAP-2 consistent with the NMR data is shown in Fig. 4, and their average is depicted as a ribbon diagram (Fig. 5*A*) and a space-filling model (Fig. 5*B*). The entire polypeptide chain has been traced except for the disordered region at the carboxyl

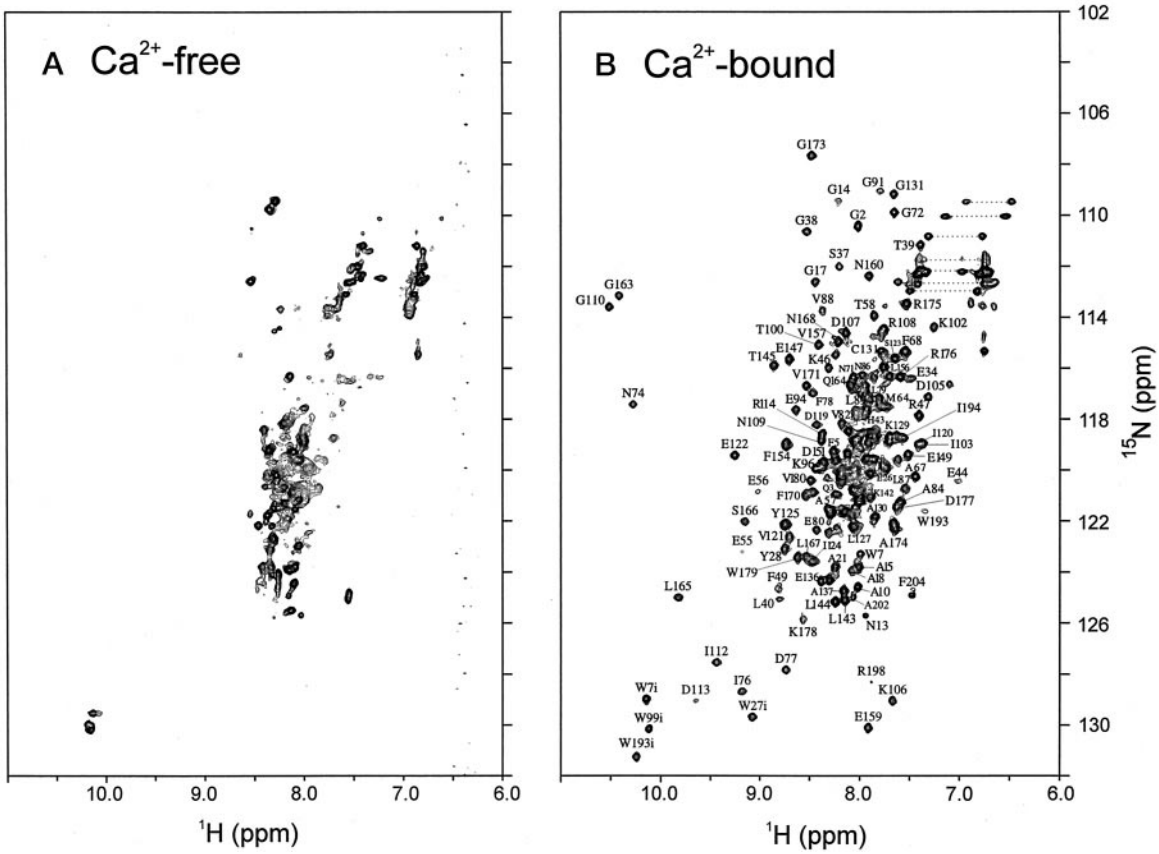

FIG. 2. **Two-dimensional NMR (^{15}N-^{1}H HSQC) spectra of Ca^{2+}-free (*A*) and Ca^{2+}-bound (*B*) unmyristoylated GCAP-2 recorded at a 500-MHz ^{1}H frequency.** Side chain resonances of Gln and Asn NH_2 groups are connected by *dotted lines*. Sequence-specific assignments of backbone amide resonances are indicated.

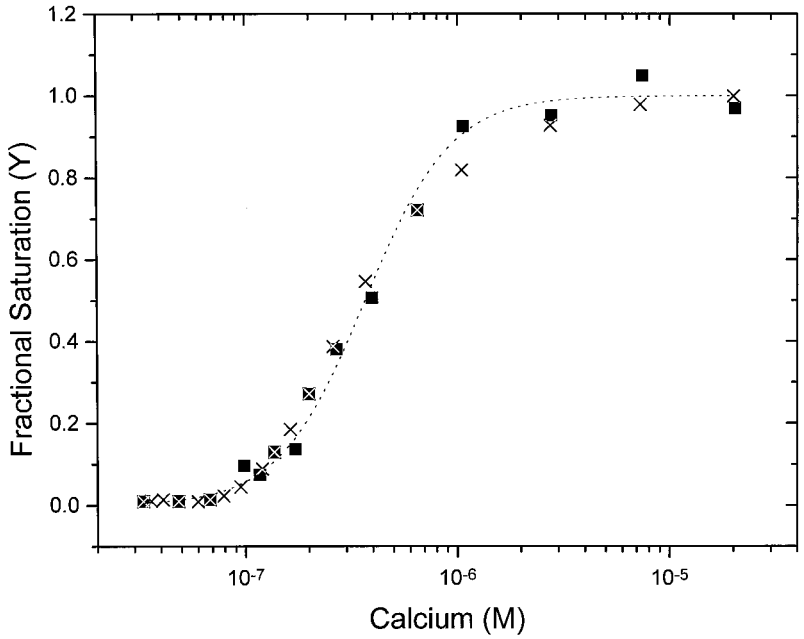

FIG. 3. **Ca^{2+}-binding curves of unmyristoylated GCAP-2 (*filled squares*) obtained by equilibrium dialysis.** The *dotted line* represents the best fit to the Hill model using an apparent dissociation constant of 300 nM and a Hill coefficient of 2.1. The points indicated with an *X* show the relative change in tryptophan fluorescence emission at 340 nm (excitation at 290 nm) as a function of Ca^{2+} concentration.

terminus (residues 191–204). The structure near the amino terminus (residues 2–18) and the region between EF-3 and EF-4 (residues 132–144) are rather poorly defined (the RMS deviation of the main chain atoms is greater than 2 Å) because of a relatively small number of nuclear Overhauser effect contacts observed in these regions. Also, chemical shift data indicate a structurally disordered, random coil secondary structure in most of these regions.

GCAP-2 is a compact protein (radius of gyration, 17 Å) made of two domains separated by a flexible linker (Fig. 5). Each domain contains a pair of EF-hands, the 29-residue helix-loop-helix motifs (highlighted in color in Fig. 1) found in calmodulin, troponin C, parvalbumin, recoverin, and other members of the superfamily (39). The EF-hands are defined from the amino terminus: EF-1 (Ala^{22}-Val^{51}), EF-2 (Thr^{58}-Leu^{87}), EF-3 (Leu^{96}-Lys^{126}), and EF-4 (Glu^{147}-Arg^{176}). EF-1 and EF-2 interact in-

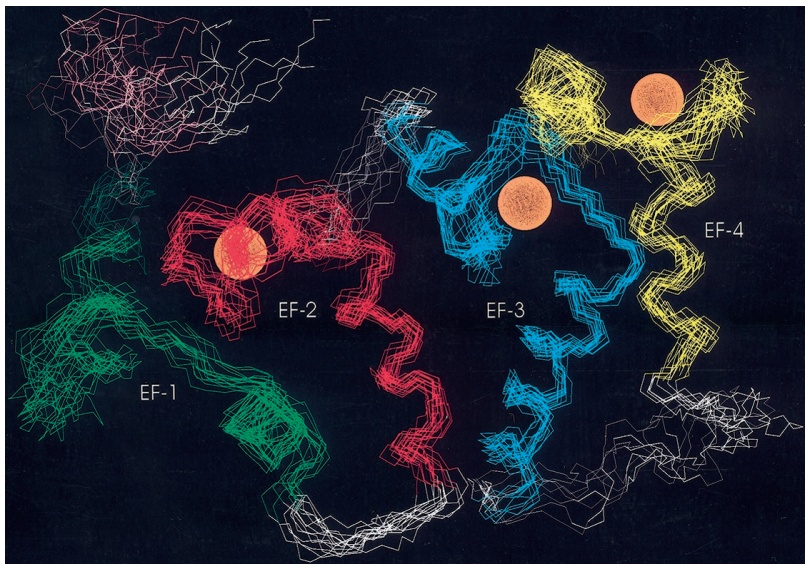

FIG. 4. **Superposition of the main chain atoms of 22 NMR-derived structures of unmyristoylated GCAP-2 with three Ca^{2+} bound.** The four EF-hands (*green, red, cyan, yellow*) and three bound Ca^{2+} (*orange*) are highlighted. The RMS deviation of the NMR-derived structures relative to the mean structure is 0.88 ± 0.1 Å for main chain atoms and 1.44 ± 0.1 Å for all non-hydrogen atoms in the regions of regular secondary structure. This figure was generated by MIDAS (48).

timately to form the NH_2-terminal domain, and EF-3 and EF-4 form the COOH-terminal domain. The entering helix of EF-2 (residues 58–68) packs against the helices of EF-3 (residues 96–104 and 114–127) at the interface between the two domains forming a cleft. Two additional α-helices occur near the amino terminus (residues 7–13) and carboxyl terminus (residues 180–186). There are two pairs of short β-strands at the interfaces between pairs of EF-hands (β-strands are located at residues 39–41 (EF-1), 75–77 (EF-2), 111–113 (EF-3), and 164–166 (EF-4)). The linker between the domains is U-shaped, which positions the four EF-hands in a compact tandem array like that found in recoverin and unlike the dumbbell arrangement found in calmodulin (35) and troponin C (40). Indeed, the overall folding of Ca^{2+}-bound unmyristoylated GCAP-2 closely resembles that of Ca^{2+}-bound unmyristoylated recoverin (24), Ca^{2+}-bound myristoylated recoverin (25), and the very recent crystal structure of Ca^{2+}-bound unmyristoylated neurocalcin (36). A superposition of the main chain structures of unmyristoylated, Ca^{2+}-bound GCAP-2 (*red*), recoverin (*blue*), and neurocalcin (*green*) are shown in Fig. 6. The RMS deviation of the main chain atoms (in the EF-hand motifs) is 2.2 Å in comparing GCAP-2 to recoverin and 2.0 Å in comparing GCAP-2 to neurocalcin.

Three Ca^{2+} are bound to GCAP-2, as anticipated on the basis of its amino acid sequence and site-directed mutagenesis. The structure of EF-3 is strikingly similar to that of EF-3 in Ca^{2+}-bound recoverin and calmodulin. The RMS deviations of the 116 main chain atoms of EF-3 are 0.66 Å in comparing GCAP-2 with recoverin and 0.80 Å in comparing GCAP-2 with calmodulin. Likewise, the coordination of Ca^{2+} is virtually identical in all three. The interhelical angle or helix packing angle of EF-3 is 94° (GCAP-2), 95° (recoverin), and 96° (calmodulin).

The structures of EF-1, EF-2, and EF-4 from GCAP-2 are somewhat different from the corresponding EF-hands of recoverin. The RMS deviations of the main chain atoms of these EF-hands are 1.9 Å (EF-1), 1.4 Å (EF-2), and 1.9 Å (EF-4) in comparing GCAP-2 with recoverin. The interhelical angles are 108° (EF-1), 109° (EF-2), and 98° (EF-4) for GCAP-2 compared with 115° (EF-2), 118° (EF-3), and 92° (EF-4) for Ca^{2+}-bound recoverin. The four EF-hands of GCAP-2 assume the "open conformation" of Ca^{2+}-occupied EF-hands seen in recoverin, calmodulin, and troponin C.

The structures of the 12-residue Ca^{2+}-binding loop of the EF-hands are depicted in Fig. 7. The loop of EF-1 is quite similar to that of recoverin and again shows why this motif does not bind Ca^{2+}. EF-1 is distorted from a favorable Ca^{2+}-binding geometry by Pro^{36} at the fourth position of the 12-residue loop. Also, the third residue in the loop (Cys^{35}) is not suitable for ligating Ca^{2+}. The bulky sulfhydryl group sterically blocks the entry of Ca^{2+}. The EF-2 loop adopts a favorable structure for binding Ca^{2+}, despite the tight turn centered at Asn^{74} (position 6 of the loop). Normally, a glycine residue is conserved at position 6 in most other EF-hands (Fig. 1). The loop of EF-3 is very typical of Ca^{2+}-occupied EF-hands and closely resembles the EF-3 loop of recoverin and calmodulin. The EF-4 loop of GCAP-2 is quite different from that of recoverin. In recoverin, the second residue in the loop (Lys^{161}) forms a salt bridge with residue 12 (Glu^{171}) that disables Ca^{2+} binding. In GCAP-2, the second residue of the EF-4 loop (Glu^{159}) is negatively charged and cannot form a salt bridge that would impede Ca^{2+} binding. Furthermore, residues 1 and 3 of the EF-4 loop (Asp^{158} and Asn^{160}) contain oxygen atoms in their side chains that can ligate Ca^{2+}, in contrast with the corresponding residues of recoverin (Gly^{160} and Lys^{162}). Thus, Ca^{2+} binds to EF-4 similarly to EF-2 and EF-3.

GCAP-2 has a solvent-exposed, hydrophobic surface formed by residues from EF-1 and EF-2 (Fig. 8*A*). The exposed patch of hydrophobic residues is formed by the clustering of several aromatic side chains (Trp^{27}, Phe^{31}, Phe^{45}, Phe^{48}, Phe^{49}, and Tyr^{81}) and several aliphatic residues (Leu^{24}, Leu^{40}, Ile^{76}, Val^{82}, Leu^{85}, and Leu^{89}) (Fig. 8*B*). These exposed hydrophobic residues are highly conserved in members of the family (22) and form a similar nonpolar patch in Ca^{2+}-bound recoverin (24, 25). In Ca^{2+}-free recoverin, these residues make close contacts with the highly sequestered myristoyl group (26). Ca^{2+}-induced extrusion of the myristoyl group causes these residues to become solvent exposed, suggesting that they may serve as a target-binding site.

DISCUSSION

In this study we present the three-dimensional structure of unmyristoylated GCAP-2 with three Ca^{2+} bound. This structure is an important step toward 1) understanding the regulatory mechanism of photoreceptor guanylyl cyclases and 2) elucidating the novel membrane-targeting mechanism of GCAPs. Although the precise structure of the amino-terminal myristoyl group of GCAP-2 could not be studied, our structure shows the amino-terminal region (residues 2–18) to be solvent exposed, suggesting that the covalently attached myristoyl group may be extruded as in Ca^{2+}-bound recoverin (25). Recent NMR

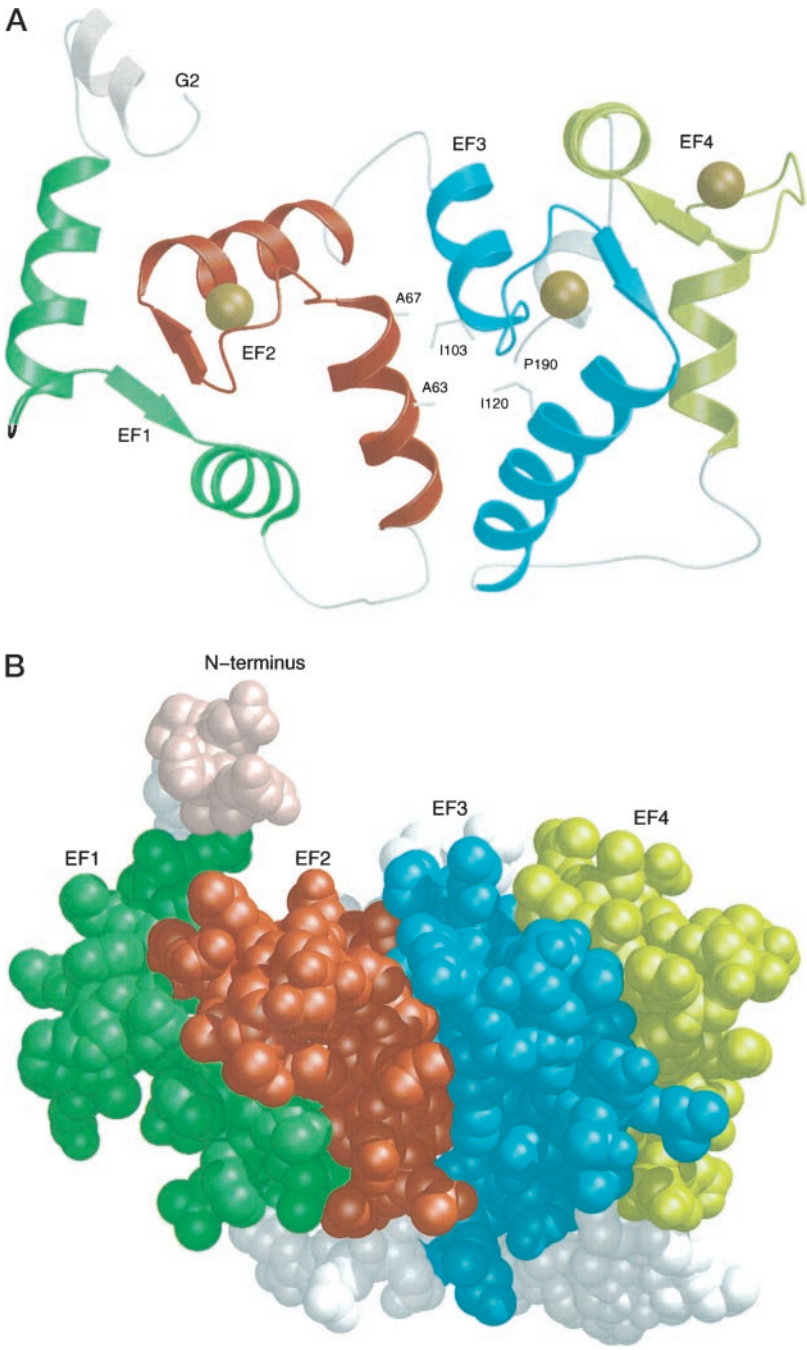

FIG. 5. **Schematic ribbon representation (*A*) and space-filling model (*B*) of the energy-minimized average structure of unmyristoylated GCAP-2 with three Ca^{2+} bound.** The side chain atoms of residues at the domain interface (Ala^{63}, Ala^{67}, Ile^{103}, and Ile^{120}) are shown in *A* and the color scheme is as in Fig. 4. The figure was generated using Molscript (49) and Raster3d (23).

studies on the myristoyl group of GCAP-2 also suggest that the myristoyl group may be solvent exposed (41). An extruded myristoyl group of Ca^{2+}-bound GCAP-2 may not necessarily interact with bilayer membranes (as demonstrated for recoverin), because the Ca^{2+}-bound, myristoylated GCAP-2 appears to be cytosolic at low ionic strength (29). Instead, the myristoyl group of GCAP-2 might interact with the cyclase or perhaps with itself to form a soluble dimer. Structural studies of the myristoylated GCAPs are needed to more rigorously determine the structural role of the myristoyl group and to test whether the myristoyl group can be sequestered in Ca^{2+}-free GCAP-2 as was seen for Ca^{2+}-free recoverin (26).

The exposed hydrophobic patch of GCAP-2 (Fig. 8) may serve a role in regulating guanylyl cyclase. Recent site-directed mutagenesis studies reveal that many of these exposed residues are important in the cyclase interaction (42). In particular, replacement of residues 78–110 (that includes the exiting helix of EF-2) with corresponding residues of neurocalcin results in a chimeric protein that fails to inhibit guanylyl cyclase at low Ca^{2+} levels but activates it at high Ca^{2+}. Also, the replacement of residues in EF-1 (residues 24–49) with the corresponding residues of neurocalcin renders the chimera completely inactive. It will be interesting to make point mutations of individual residues in the exposed patch to more precisely map their effect on the cyclase interaction.

The hydrophobic patch of GCAP-2 may also serve as a possible dimerization site. The crystal structures of Ca^{2+}-bound unmyristoylated recoverin (24) and neurocalcin (36) both show the presence of a stable dimer in the asymmetric unit. Dimerization of GCAP-2 might enable a Ca^{2+}-bound monomer to tie up a Ca^{2+}-free monomer to prevent activation of the cyclase. Alternatively, a dimer of Ca^{2+}-bound GCAP-2 might bind directly to the cyclase and inhibit it. However, GCAP-2 does not appear to dimerize in our NMR experiments perhaps because

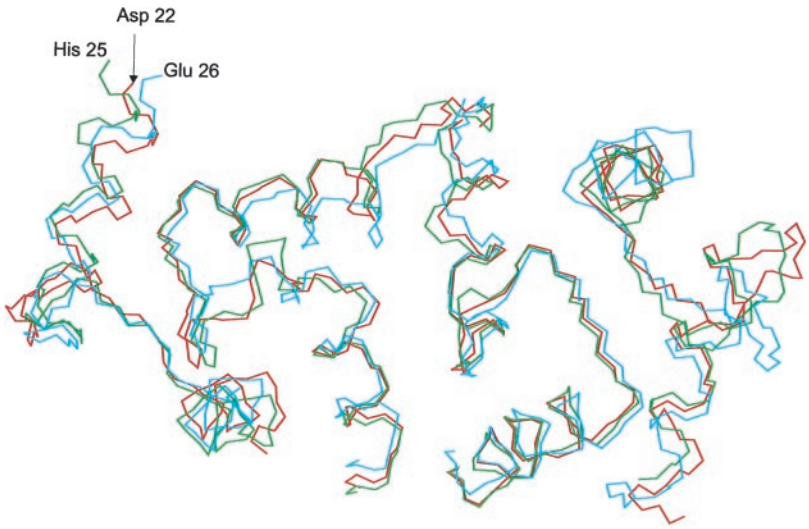

FIG. 6. **Superposition of the main chain structures of the EF-hand motifs of Ca^{2+}-bound unmyristoylated GCAP-2 (*red*), recoverin (*blue*, 1jsa.pdb), and neurocalcin (*green*, 1bjf.pdb).**

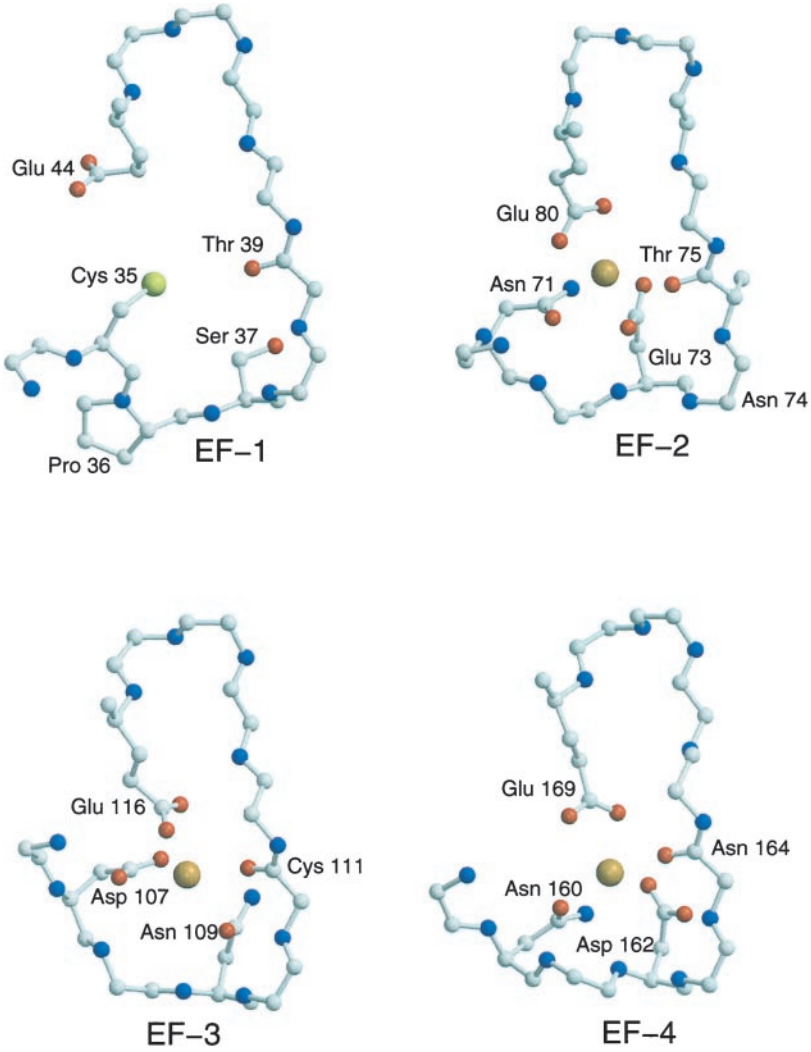

FIG. 7. **Ball-and-stick models of the 12-residue loops of the four EF-hands of GCAP-2.** Bound Ca^{2+} is shown in *orange*. Oxygen, nitrogen, and sulfur are *red*, *blue*, and *yellow*, respectively. Side chain atoms are shown for the residues that ligate Ca^{2+}.

detergent (20 mM octyl glucoside) was present in our samples to dramatically sharpen the peaks in the NMR spectrum. This detergent does not appear to denature or inactivate GCAP-2 as was demonstrated in the original purification of GCAP-2 from the retina.[3] Additional studies are needed to test whether GCAP-2 forms a functional dimer under physiological conditions.

The structure of GCAP-2 near the amino terminus (residues 2–18) appears different from that of recoverin. There is virtually no sequence similarity between recoverin and the GCAPs in this region. Recoverin contains a long, amphipathic helix (residues 4–18) that packs against the sequestered myristoyl group (26). This amino-terminal helix is considerably shorter in bovine GCAP-2 (residues 7–13) because four residues have been deleted in this region (Fig. 1). The orientation of the

[3] A. M. Dizhoor, personal communication.

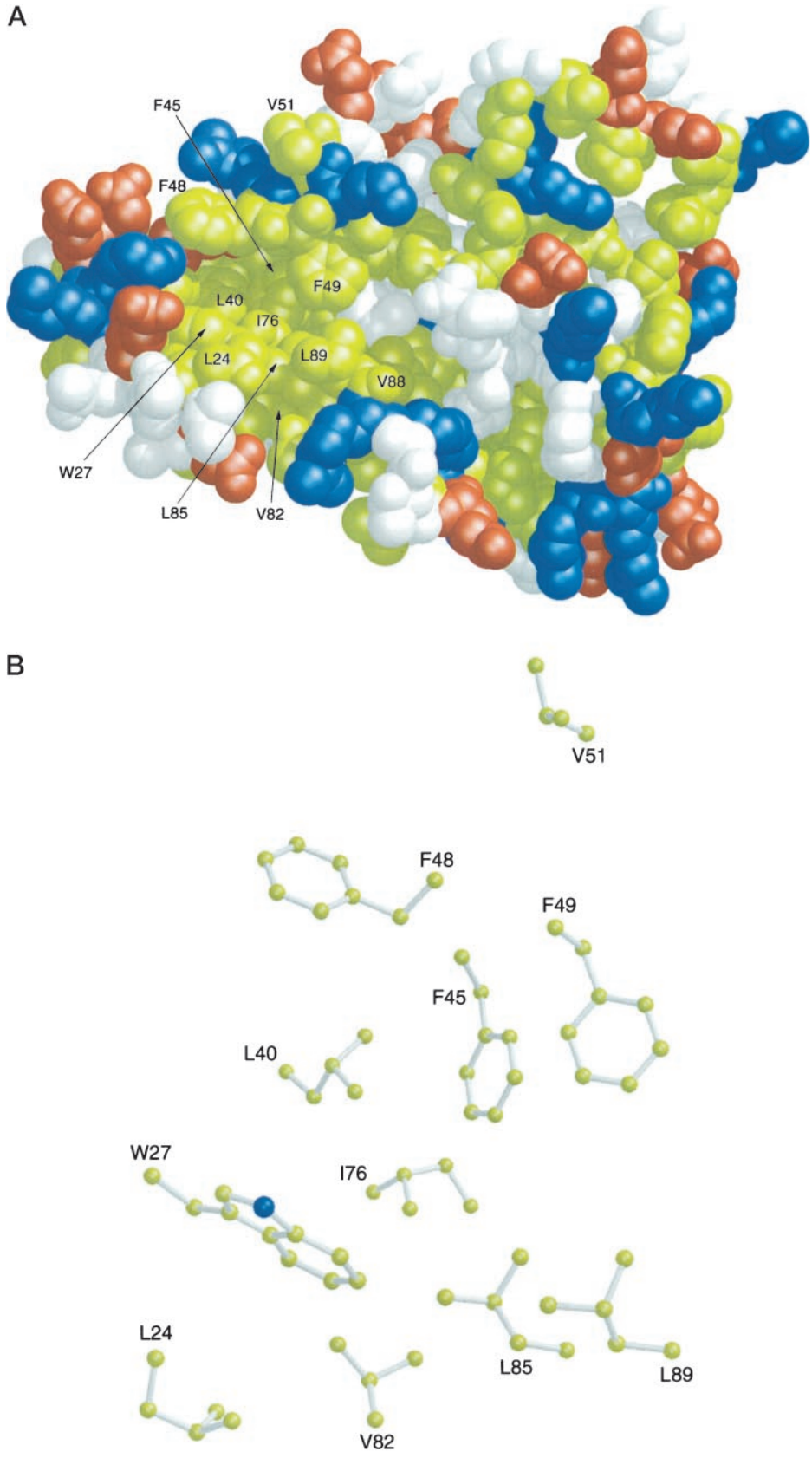

FIG. 8. **Space-filling representation (*A*) and ball-and-stick model (*B*) of side chain atoms of the exposed hydrophobic patch of GCAP-2.** Hydrophobic, negatively charged, and positively charged residues are highlighted in *yellow*, *red*, and *blue*, respectively. Solvent-exposed hydrophobic residues from EF-1 and EF-2 are indicated.

amino-terminal helix is different in recoverin and GCAP-2. This helix in recoverin extends close to the interdomain linker, whereas it interacts primarily with the entering helix of EF-1 in GCAP-2. The helix orientation in GCAP-2 is also characterized by contacts between Ser^{6} and Leu^{79}. We note, however, that these apparent structural differences in the amino-terminal region between recoverin and GCAP-2 may result from the very low precision of our structure in this region (RMS deviation, 4 Å) because of dynamical disordering. Substitution of this amino-terminal region with the corresponding residues of neurocalcin has little effect on the function of GCAP-2 (42), consistent with our finding that this region is structurally

disordered.

The carboxyl-terminal helix (residues 180–186, highlighted in *white* in Fig. 5) interacts with the helices of EF-3 and EF-4, similar to that seen for recoverin (43). The association of the COOH-terminal helix with these EF-hands resembles the interaction of calmodulin with its helical target peptides (44). The carboxyl-terminal helix may enhance the specificity of GCAP-2 and recoverin by blocking their adventitious binding to targets of calmodulin.

The GCAP-2 structure is likely to be similar to that of GCAP-1 (40% sequence identity), GCAP-3 (35% identity), and GCIP (37% identity), because the overall main chain structure appears so similar to recoverin (RMS deviation, 2.2 Å; identity, 30%) and to neurocalcin (RMS deviation, 2.0 Å; identity, 40%). Most of the hydrophobic residues in the hydrophobic core and in the exposed patch (Fig. 8) are highly conserved. Also conserved are the residues that ligate Ca^{2+} in the EF-hand loops (Fig. 7). Interestingly, important residues in the entering helix of EF-2 at the domain interface (Ala^{57}, Ala^{63}, and Ala^{67}) are not conserved. Other structurally important and nonconserved residues include Asn^{74}, Leu^{79}, Thr^{93}, His^{95}, and Thr^{100}. Considerable differences are also found in the amino-terminal (residues 2–18) and carboxyl-terminal (residues 191–204) regions. These differences suggest that the interaction and/or orientation between the NH_2-terminal and COOH-terminal domains might be different in GCAP-1, GCAP-3, and GCIP. Indeed, a point mutation at the domain interface causes very different phenotypes in GCAP-1 and GCAP-2. The mutation (Y99C) causes GCAP-1 to be constitutively active (45, 46), resulting in autosomal dominant cone dystrophy in humans (47). In contrast, the corresponding mutation in GCAP-2 (Y104C) does not alter its Ca^{2+} sensitivity and partially inactivates GCAP-2 (45).

In summary, we have determined the structure of unmyristoylated GCAP-2 with three bound Ca^{2+} by NMR spectroscopy. The overall main chain structure of GCAP-2 is similar to that of Ca^{2+}-bound recoverin except for structural differences near the amino terminus (residues 2–18) and the binding of Ca^{2+} to EF-4. We see an exposed hydrophobic patch of residues belonging to EF-1 and EF-2 that may play a role in regulating guanylyl cyclase. Our next goal is to solve the structure of Ca^{2+}-free GCAP-2, a formidable challenge because of its lower stability and solubility, to fully elucidate the Ca^{2+}-induced structural changes that enable GCAP-2 to activate guanylyl cyclases in the absence of Ca^{2+}.

Acknowledgments—We thank L. Kay for help with NMR experiments, C. Vain for preparing samples of GCAP-2, F. Delaglio and D. Garrett for writing computer software for NMR data processing and analysis, and Vinod D. Kumar for providing coordinates of neurocalcin.

REFERENCES

1. Baylor, D. (1996) *Proc. Natl. Acad. Sci. U. S. A.* **93,** 560–565
2. Polans, A., Baehr, W., and Palczewski, K. (1996) *Trends Neurosci.* **19,** 547–554
3. Stryer, L. (1991) *J. Biol. Chem.* **266,** 10711–10714
4. Yarfitz, S., and Hurley, J. B. (1994) *J. Biol. Chem.* **269,** 14329–14332
5. Gray-Keller, M. P., and Detwiler, P. B. (1994) *Neuron* **13,** 849–861
6. Ratto, G. M., Payne, R., Owen, W. G., and Tsien, R. Y. (1988) *J. Neurosci.* **8,** 3240–3246
7. Sampath, A. P., Matthews, H. R., Cornwall, M. C., and Fain, G. L. (1998) *J. Gen. Physiol.* **111,** 53–64
8. Koutalos, Y., and Yau, K. W. (1996) *Trends. Neurosci.* **19,** 73–81
9. Koch, K. W., and Stryer, L. (1988) *Nature* **334,** 64–66
10. Lowe, D. G., Dizhoor, A. M., Liu, K., Gu, Q., Laura, R., Lu, L., and Hurley, J. B. (1995) *Proc. Natl. Acad. Sci. U. S. A.* **92,** 5535–5539
11. Shyjan, A. W., de Sauvage, F. J., Gillet, N. A., Goeddel, D. V., and Lowe, D. G. (1992) *Neuron* **9,** 727–737
12. Yang, R. B., Foster, D. C., Garbers, D. L., and Fulle, H. J. (1995) *Proc. Natl. Acad. Sci. U. S. A.* **92,** 602–606
13. Palczewski, K., Subbaraya, I., Gorczyca, W. A., Helekar, B. S., Ruiz, C. C., Ohguro, H., Huang, J., Zhao, X., Crabb, J. W., Johnson, R. S., Walsh, K. A., Gray-Keller, M. P., Detwiler, P. B., and Baehr, W. (1994) *Neuron* **13,** 395–404
14. Dizhoor, A. M., Lowe, D. G., Olshevskaya, E. V., Laura, R. P., and Hurley, J. B. (1994) *Neuron* **12,** 1345–1352
15. Haeseleer, F., Sokal, I., Li, N., Pettenati, M., Nagesh, R., Bronson, D., Wechter, R., Baehr, W., and Palczewski, K. (1999) *J. Biol. Chem.* **274,** 6526–6535
16. Dizhoor, A. M., and Hurley, J. B. (1996) *J. Biol. Chem.* **271,** 19346–19350
17. Li, N., Fariss, R. N., Zhang, K., Otto-Bruc, A., Haeseleer, F., Bronson, D., Qin, N., Yamazaki, A., Subbaraya, I., Milam, A. H., Palczewski, K., and Baehr, W. (1998) *Eur. J. Biochem.* **15,** 591–599
18. Ikura, M. (1996) *Trends Biochem. Sci.* **1,** 14–17
19. Dizhoor, A. M., Ray, S., Kumar, S., Niemi, G., Spencer, M., Brolley, D., Walsh, K. A., Philipov, P. P., Hurley, J. B., and Stryer, L. (1991) *Science* **251,** 915–918
20. Chen, C. K., Inglese, J., Lefkowitz, R. J., and Hurley, J. B. (1995) *J. Biol. Chem.* **270,** 18060–18066
21. Klenchin, V. A., Calvert, P. D., and Bownds, M. D. (1995) *J. Biol. Chem.* **270,** 16147–16152
22. Ames, J. B., Tanaka, T., Stryer, L., and Ikura, M. (1996) *Curr. Opin. Struct. Biol.* **6,** 432–438
23. Bacon, D. J., and Anderson, W. F. (1988) *J. Mol. Graph.* **6,** 219–220
24. Flaherty, K. M., Zozulya, S., Stryer, L., and McKay, D. B. (1993) *Cell* **75,** 709–716
25. Ames, J. B., Ishima, R., Tanaka, T., Gordon, J. I., Stryer, L., and Ikura, M. (1997) *Nature* **389,** 198–202
26. Tanaka, T., Ames, J. B., Harvey, T. S., Stryer, L., and Ikura, M. (1995) *Nature* **376,** 444–447
27. Zozulya, S., and Stryer, L. (1992) *Proc. Natl. Acad. Sci. U. S. A.* **89,** 11569–11573
28. Dizhoor, A. M., Chen, C. K., Olshevskaya, E., Sinelnikova, V. V., Phillipov, P., and Hurley, J. B. (1993) *Science* **259,** 829–832
29. Olshevskaya, E. V., Hughes, R. E., Hurley, J. B., and Dizhoor, A. M. (1997) *J. Biol. Chem.* **272,** 14327–14333
30. Tanaka, T., Ames, J. B., Kainosho, M., Stryer, L., and Ikura, M. (1998) *J. Biomol. NMR* **11,** 135–152
31. Ames, J. B., Tanaka, T., Stryer, L., and Ikura, M. (1994) *Biochemistry* **33,** 10743–10753
32. Nilges, M., Gronenborn, A. M., Brunger, A. T., and Clore, G. M. (1988) *Protein Eng.* **2,** 27–38
33. Brunger, A. T. (1992) *X-PLOR Version 3.1: A System for X-ray Crystallography and NMR*, Yale University Press, New Haven, CT
34. Bagby, S., Harvey, T. S., Eagle, S. G., Inouye, S., and Ikura, M. (1994) *Structure* **2,** 107–122
35. Babu, Y. S., Bugg, C. E., and Cook, W. J. (1988) *J. Mol. Biol.* **204,** 191–199
36. Vijay-Kumar, S., and Kumar, V. D. (1999) *Nat. Struct. Biol.* **6,** 80–88
37. Brooks, S. P. J., and Storey, K. B. (1992) *Anal. Biochem.* **201,** 119–126
38. Tsien, R., and Pozzan, T. (1989) *Methods Enzymol.* **172,** 230–262
39. Moncrief, N. D., Kretsinger, R. H., and Goodman, M. (1990) *J. Mol. Evol.* **30,** 522–562
40. Herzberg, O., and James, M. N. (1985) *Nature* **313,** 653–659
41. Hughes, R. E., Brzovic, P. S, Dizhoor, A. M., Klevit, R. E., and Hurley, J. B. (1998) *Protein Sci.* **7,** 2675–2680
42. Olshevskaya, E. V., Boikov, S., Ermilov, A., Krylov, D., Hurley, J. B., and Dizhoor, A. M. (1999) *J. Biol. Chem.* **274,** 10823–10832
43. Yap, K., Ames, J. B, Swindells, M., and Ikura, M. (1999) *Trends Biochem. Sci.*, in press
44. Ikura, M., Clore, G. M., Gronenborn, A. M., Zhu, G., Klee, C. B., and Bax, A. (1992) *Science* **256,** 632–638
45. Dizhoor, A. M., Boikov, S. G., and Olshevskaya, E. V. (1998) *J. Biol. Chem.* **273,** 17311–17314
46. Sokal, I., Li, N., Surgucheva, I., Warren, M. J., Payne, A. M., Bhattacharya, S. S., Baehr, W., and Palczewski, K. (1998) *Mol. Cell* **2,** 129–133
47. Payne, A. M., Downes, S. M., Bessant, D. A. R., Taylor, R., Holder, G. E., Warren, M. J., Bird, A. C., and Bhattacharya, S. S. (1998) *Hum. Mol. Genet.* **7,** 273–277
48. Ferrin, T., Huang, C., Jarvis, L., and Langridge, R. (1988) *J. Mol. Graph.* **6,** 13–27
49. Kraulis, P. J. (1991) *J. Appl. Crystallogr.* **24,** 946–950